Appl. Math. Mech. -Engl. Ed., **43**(9), 1399–1414 (2022)

APPLIED MATHEMATICS AND MECHANICS (ENGLISH EDITION)

https://doi.org/10.1007/s10483-022-2896-7

Regulating absence seizures by tri-phase delay stimulation applied to globus pallidus internal*

Songan HOU[1], Denggui FAN[2], Qingyun WANG[1,3,†]

1. Department of Dynamics and Control, Beihang University, Beijing 100191, China;
2. School of Mathematics and Physics, University of Science and Technology Beijing, Beijing 100083, China;
3. Beijing Institute of Brain Disorders, Capital Medical University, Beijing 100069, China

(Received May 22, 2022 / Revised Jun. 15, 2022)

Abstract In this paper, a reduced globus pallidus internal (GPI)-corticothalamic (GCT) model is developed, and a tri-phase delay stimulation (TPDS) with sequentially applying three pulses on the GPI representing the inputs from the striatal D_1 neurons, subthalamic nucleus (STN), and globus pallidus external (GPE), respectively, is proposed. The GPI is evidenced to control absence seizures characterized by 2 Hz–4 Hz spike and wave discharge (SWD). Hence, based on the basal ganglia-thalamocortical (BGCT) model, we firstly explore the triple effects of D_1-GPI, GPE-GPI, and STN-GPI pathways on seizure patterns. Then, using the GCT model, we apply the TPDS on the GPI to potentially investigate the alternative and improved approach if these pathways to the GPI are blocked. The results show that the striatum D_1, GPE, and STN can indeed jointly and significantly affect seizure patterns. In particular, the TPDS can effectively reproduce the seizure pattern if the D_1-GPI, GPE-GPI, and STN-GPI pathways are cut off. In addition, the seizure abatement can be obtained by well tuning the TPDS stimulation parameters. This implies that the TPDS can play the surrogate role similar to the modulation of basal ganglia, which hopefully can be helpful for the development of the brain-computer interface in the clinical application of epilepsy.

Key words epileptic absence seizure, spike and wave discharge (SWD), tri-phase delay stimulation (TPDS), mean field model, seizure control

Chinese Library Classification O175, O322
2010 Mathematics Subject Classification 37H20, 37N25, 34D10, 34D20

1 Introduction

Absence epilepsy is a kind of generalized epilepsy with the hallmark of abrupt and brief impairment of the patients' consciousness, interrupting the ongoing activity and causing unresponsiveness. Always, the absence epilepsy lasts for a few to 20 seconds and ends with a

* Citation: HOU, S. A., FAN, D. G., and WANG, Q. Y. Regulating absence seizures by tri-phase delay stimulation applied to globus pallidus internal. *Applied Mathematics and Mechanics* (*English Edition*), **43**(9), 1399–1414 (2022) https://doi.org/10.1007/s10483-022-2896-7

† Corresponding author, E-mail: nmqingyun@163.com

Project supported by the National Natural Science Foundation of China (Nos. 11932003, 12072021, and 11672074)

sudden resumption from the absence[1–4]. With the electrophysiological techniques, the mechanism of the absence seizure has been preliminarily explored. The occurrence of the absence epilepsy is related to the abnormal interactions between the cortex and the thalamus[5–8]. This kind of view can be directly supported by the recordings of the electroencephalogram of the thalamus and the cortex in rodent animal experiments and clinical patients[9–11]. The seizure of the absence epilepsy is characterized by the hallmarks of bilaterally synchronous spike and wave discharge (SWD) with a low frequency of 2 Hz–4 Hz. Nowadays, there are many studies on the computational model of the seizures about the corticothalamic system to go deep into the potential reasons for the generation of the absence seizures and to offer instruction for the treatment of this disease[12–19].

Basal ganglia is evidenced to modulate the absence seizures by bridging the communications between cortex and thalamus through the direct, indirect, and hyperdirect pathways of basal ganglia[20–22]. Hence, many computational models of the basal ganglia-corticothalamic (BGCT) circuit have been developed to investigate the seizure control. The globus pallidus internal (GPI) is the main output of the basal ganglia. It converges the signals from the striatal D_1 neurons, subthalamic nucleus (STN), and globus pallidus external (GPE), respectively. Based on the BGCT model, Chen et al.[19] and Deransart et al.[20] computationally demonstrated that the GPI can bidirectionally control seizures due to the competition between the inhibitory GPI to the thalamic reticular nucleus (TRN) and to the specific relay nuclei (SRN) of the thalamus. Hence, it can be inferred that the control effect might be affected by the D_1-GPI, GPE-GPI, and STN-GPI pathways. However, there is no literature referring to how the control of GPI for seizures can be maintained or repaired if the basal ganglia shows dysregulation, i.e., the input pathways to GPI are blocked or broken. For this purpose, we will reduce the BGCT model by discarding the D_1-GPI, GPE-GPI, and STN-GPI pathways and propose a simplified GPI-corticothalamic (GCT) model to simulate the dysregulation of basal ganglia.

For the treatment of absence seizures, medicine is the main method to stop the seizures[23–25]. However, there are patients who show resistance to antiepileptic medications[26]. Meanwhile, although focal removal is another way to abate the absence seizures, it could lead to more risk to the patients. Deep brain stimulation (DBS) has been widely applied in the field of treatment of the diseases of the nervous system[27]. Specific stimulation can depress or control the seizures or other diseases of the nervous system, which has been proven by electrophysiological and clinical experiments[27–32].

The forms and methods of DBS have evolved greatly because of the initialization of stimulation, and recent results have combined multiple strategies and perspectives to improve the control of epilepsy, such as the optimization of stimulation parameters to achieve better or new control effects[33–34]; continuous exploration of space target locations and strategies of the combination of targets[35]; new stimulus ideas such as agent stimulus[36]; the combination of stimulus effects with control theory and optimization theory[33, 37]. In particular, the stimulation parameters, such as the stimulation frequency, stimulation amplitude, and stimulation pulse width, can be adjusted to change the control effect of seizures. In addition, the stimulation spatiotemporal patterns can also be flexibly redesigned to improve seizure control[38–39]. This suggests that it is potentially feasible to consider the optimized stimulation as a remedial measure of abnormal inputs of the STN, GPE, and striatal D_1 neurons to GPI. This is also the key issue of this paper.

It is electrophysiologically observed that there exist significantly different information transmission delays from the D_1, GPE, and STN to GPI, the arrival times of which at GPI is 7.8 ms, 20.9 ms, and 29.9 ms (the approximate ratio of 1:3:4)[40–42], respectively. In view of this, in this paper, we will first investigate the combined effects of the D_1-GPI, GPE-GPI, and STN-GPI pathways on seizure control based on the BGCT model. Then, based on the reduced GCT model and the above electrophysiological observation, we will computationally propose a new tri-phase delay stimulation (TPDS) pattern with the interphase gap (IPG) consistent with

information transmission delays of these three pathways, to repair the dysregulation of basal ganglia for seizures and reproduce the control and modulating effect of basal ganglia. Furthermore, we will also explore the improving effect of the optimized stimulus on seizure control by using the new tri-phase stimulation. In conclusion, under the assumption that the regulation from the STN, GPE, and striatal D_1 neurons is missing, TPDS with similar signal forms to the three channels may play a similar control role in the seizure of the nervous system model, and the stimulation form of TPDS with alternating positive and negative electrodes may bring less damage compared with the monophasic stimulation. Its signal form similar to endogenous regulation may also help restore the function of impaired basal ganglia.

2 Model and method

2.1 Mathematical models of BGCT circuit and its reduced GCT model

Biophysically based models have been built for both the investigation of the role of three channels to GPI and the possible effect of stimulation[18–19], which are illustrated in Fig. 1. Figure 1(a) shows the original BGCT model consisting of nine neuronal populations which are indicated as follows: excitatory pyramidal neurons (e), inhibitory interneurons (i), thalamic reticular nucleus (TRN, r), specific relay nuclei (SRN, s), striatal D_1 neurons ($d1$), striatal D_2 neurons ($d2$), globus pallidus internal (GPI, $p1$), globus pallidus external (GPE, $p2$), and subthalamic nucleus (STN, ζ). In view of the close connection between the outputs of SNr and GPI, we also consider the two populations as a single structure of the circuit like the previous works in the literature[43–44]. Besides, in the circuit, there are a total of three types of synapse,

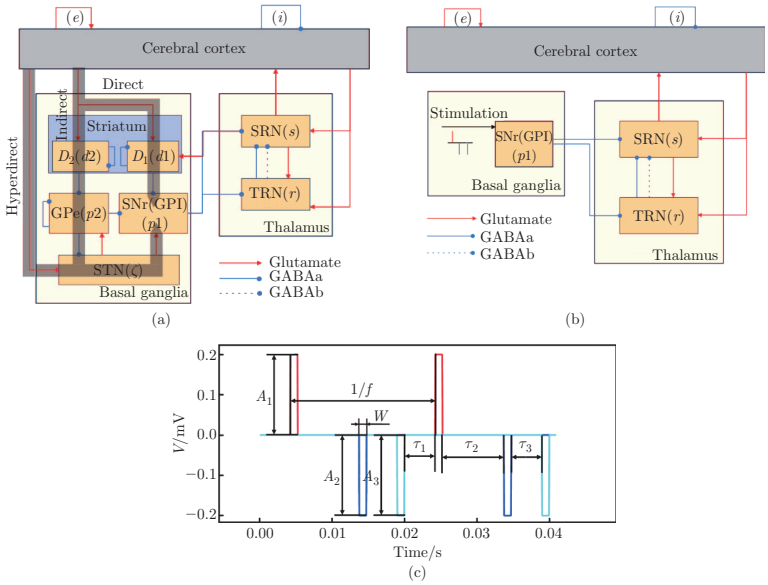

Fig. 1 Structure diagrams of BGCT and GCT models. (a) Schematic diagram of BGCT model, including cortex, thalamus, and basal ganglia. Basal ganglia consists of direct, indirect, and hyperdirect pathways indicated by gray shaded arrows. (b) Schematic diagram of GCT model, where basal ganglia is reduced to contain only GPI, on which stimulus is also applied. Synaptic connections are represented by connecting wires (arrow connection lines: glutamate excitatory connection; round head connection lines: GABA inhibitory connection; solid lines: GABAa-modulated projections; dotted lines: GABAb-modulated projections). (c) Schematic diagram of TPDS with anodic phase and two cathodic phases, where pulse delays are $\tau_1 = 4.74$ ms, $\tau_2 = 8.5$ ms, $\tau_3 = 4.75$ ms, being ratio of 1:2:1, which is consistent with transmission delays of $1{:}3{:}4 = \tau_1 : (\tau_1 + \tau_2) : (\tau_1 + \tau_2 + \tau_3)$. A_1, A_2, and A_3 are pulse amplitudes, W is pulse width, and f is frequency of TPDS (color online)

of which, one is excitatory projection modulated by the glutamate and the other two inhibitory projections controlled by the GABAa and GABAb.

The specific connection between the populations has been proved by Refs. [16], [18]–[19], [43]–[45], and [49], and the connections modulated by the GABAa fast dynamic and GABAb slow dynamic mechanism between the TRN and SRN are the crucial factors in the occurrence of seizures.

To model the dynamics of neuronal populations, the mean-field model is used to describe activities of each population, which represent the local mean value of the populations[16,18–19,43–49]. For each population, the mean firing rate $Q_a(\boldsymbol{r},t)$ can be acquired by an increasing sigmoid function of the mean membrane potential $V_a(\boldsymbol{r},t)$, i.e., $Q_a(\boldsymbol{r},t)=SV_a(\boldsymbol{r},t)$, given by[16,18–19,43–49]

$$Q_a(\boldsymbol{r},t)\equiv S(V_a(\boldsymbol{r},t))=\frac{Q_a^{\max}}{1+\exp\Big(-\frac{\pi}{\sqrt{3}}\frac{(V_a(\boldsymbol{r},t)-\theta_a)}{\sigma}\Big)}, \tag{1}$$

where the subscript a refers to the nine different neuronal populations, $Q_a^{\max}$ is the maximum mean firing rate, σ is the standard deviation of the mean firing rate, and the interpretations and values for other parameters can be found in Table 1.

In addition, each population receives weighted synapse inputs $v_{ab}\cdot\phi_b(\boldsymbol{r},t)$ from population b. Therein, v_{ab} represents the coupling strength from the presynaptic neuronal population b to the postsynaptic neuronal population a, where for the excitatory connections, v_{ab} is positive, while v_{ab} is negative when the synapses are inhibitory connection. $\phi_b(\boldsymbol{r},t)$ corresponds to the propagating axonal field of the presynaptic population b at the position $\boldsymbol{r}$ and at the time t. It is noted that the transmission delays among most neural populations are not considered for simplicity, while a delay parameter τ will be introduced to the incoming pulse rate $\phi_b(\boldsymbol{r},t-\tau)$ due to the GABAb functions via second messenger processes with which to describe the slow synaptic kinetics. This will result in a delay differential equation describing the BGCT model. Each neural population gives rise to a field ϕ_b which can travel to other neural populations. Then, by using the incoming pulse rate ϕ_b, the change of the mean membrane potential can be modeled by[16, 18, 19, 43–49]

$$D_{\alpha\beta}V_a(\boldsymbol{r},t)=\sum_{b\in A}v_{ab}\cdot\phi_b(\boldsymbol{r},t)+v_{\rm stim}S(t_{\rm s}), \tag{2}$$

where A is the set of different neuronal populations, $v_{\rm stim}$ is the strength parameter of stimulus, $t_{\rm s}$ is the time series of the stimulus, and $D_{\alpha\beta}$ is a differential operator,

$$D_{\alpha\beta}=\frac{1}{\alpha\beta}\Big(\frac{\partial^2}{\partial t^2}+(\alpha+\beta)\frac{\partial}{\partial t}+\alpha\beta\Big), \tag{3}$$

which represents the synaptic and dendritic filtering of the input signals, and α and β represent the decay and rise time constant of the input signals.

The transmission efficiency of ϕ_a depends on the cell-body axon. However, the cortex excitatory pyramidal cells have much longer axons than the other neuronal populations. Here, the propagation process on the axons is in the form of the dumped wave function, i.e., the change of ϕ_a can be modeled as follows[16, 18, 19, 43–49]:

$$D_a\phi_a(\boldsymbol{r},t)=Q_a(\boldsymbol{r},t), \tag{4}$$

and the operator of the spatiotemporal differential operator D_a is defined by[16, 18, 19, 43–49]

$$D_a=\frac{1}{\gamma_a^2}\Big(\frac{\partial^2}{\partial t^2}+2\gamma_a\frac{\partial}{\partial t}+\gamma_a^2-v_a^2\nabla^2\Big), \tag{5}$$

where ∇^2 is the Laplacian operator representing the second space derivative, and the γ_a is the dispersion parameter governing the dumped rate of the population a, which is defined by $\gamma_a=v_a/r_a$, where v_a is the conduction velocity parameter of the neuron population a, and r_a is

the characteristic range parameter of the population a. Since the absence epilepsy is a kind of epilepsy of generalized seizure, with the hypothesis of consistency, the term of space derivative can be ignored, i.e., $\nabla^2 = 0$. Hence, D_a can be reduced to[16, 18, 19, 47–49]

$$D_a = \frac{1}{\gamma_a^2}\Big(\frac{\partial^2}{\partial t^2} + 2\gamma_a\frac{\partial}{\partial t} + \gamma_a^2\Big). \tag{6}$$

However, it is noted that only the spatiotemporal spreading process of the cortical excitatory pyramidal cells is maintained due to their long axons. The axons of other populations are too short to support the propagation process, thus giving $\phi_a = S(V_a) = Q_a$.

The detailed equations for the BGCT model are given as follows:

$$\begin{cases}
\dfrac{\mathrm{d}^2\phi_e(t)}{\mathrm{d}t^2} = \gamma_e^2(-\phi_e(t) + S(V_e(t))) - 2\gamma_e\dot{\phi}_e(t),\\
\dfrac{\mathrm{d}^2V_e(t)}{\mathrm{d}t^2} = \alpha\beta(-V_e(t) + v_{ee}\phi_e(t) + v_{ei}S(V_e(t)) + v_{es}S(V_s(t))) - (\alpha+\beta)\dot{V}_e(t),\\
\dfrac{\mathrm{d}^2V_{d_1(t)}}{\mathrm{d}t^2} = \alpha\beta(-V_{d_1}(t) + v_{d_1e}\phi_e(t) + v_{d_1d_1}S(V_{d_1}(t)) + v_{d_1s}S(V_s(t))) - (\alpha+\beta)\dot{V}_{d_1}(t),\\
\dfrac{\mathrm{d}^2V_{d_2}(t)}{\mathrm{d}t^2} = \alpha\beta(-V_{d_2}(t) + v_{d_2e}\phi_e(t) + v_{d_2d_2}S(V_{d_2}(t)) + v_{d_2s}S(V_s(t))) - (\alpha+\beta)\dot{V}_{d_2}(t),\\
\dfrac{\mathrm{d}^2V_{p_1}(t)}{\mathrm{d}t^2} = \alpha\beta(-V_{p_1}(t)+v_{p_1d_1}S(V_{d_1}(t))+v_{p_1p_2}S(V_{p_2}(t))+v_{p_1\zeta}S(V_\zeta(t)))-(\alpha+\beta)\dot{V}_{p_1}(t),\\
\dfrac{\mathrm{d}^2V_{p_2}(t)}{\mathrm{d}t^2} = \alpha\beta(-V_{p_2}(t)+v_{p_2d_2}S(V_{d_2}(t))+v_{p_2p_2}S(V_{p_2}(t))+v_{p_2\zeta}S(V_\zeta(t)))-(\alpha+\beta)\dot{V}_{p_2}(t),\\
\dfrac{\mathrm{d}^2V_\zeta(t)}{\mathrm{d}t^2} = \alpha\beta(-V_\zeta(t) + v_{\zeta e}\phi_e(t) + v_{\zeta p_2}S(V_{p_2}(t))) - (\alpha+\beta)\dot{V}_\zeta(t),\\
\dfrac{\mathrm{d}^2V_r(t)}{\mathrm{d}t^2} = \alpha\beta(-V_r(t) + v_{re}\phi_e(t) + v_{rp_1}S(V_{p_1}(t)) + v_{rs}S(V_s(t))) - (\alpha+\beta)\dot{V}_r(t),\\
\dfrac{\mathrm{d}^2V_s(t)}{\mathrm{d}t^2} = \alpha\beta(-V_s(t) + v_{se}\phi_e(t) + v_{sp_1}S(V_{p_1}(t)) + v_{sr}^AS(V_r(t))\\
\qquad\qquad + v_{sr}^BS(V_r(t-\tau)) + \phi_n) - (\alpha+\beta)\dot{V}_s(t),
\end{cases} \tag{7}$$

where the variable τ in Eq. (7) denotes the GABAb delay.

To mimic the dysregulation of basal ganglia, the GCT model corresponding to Fig. 1(b) is developed, in which, except from GPI, other populations of basal ganglia are ignored to simulate the situation that the direct, indirect, and hyperdirect pathways to GPI fail to control the dynamic activity of GPI. And on this situation, the external stimulus can be applied to the GPI without the effect of the original internal control to investigate the mechanism of the external stimulus controlling the seizures. And the detailed equations of the GCT model are given by

$$\begin{cases}
\dfrac{\mathrm{d}^2\phi_e(t)}{\mathrm{d}t^2} = \gamma_e^2(-\phi_e(t) + S(V_e(t))) - 2\gamma_e\dot{\phi}_e(t),\\
\dfrac{\mathrm{d}^2V_e(t)}{\mathrm{d}t^2} = \alpha\beta(-V_e(t) + v_{ee}\phi_e(t) + v_{ei}S(V_e(t)) + v_{es}S(V_s(t))) - (\alpha+\beta)\dot{V}_e(t),\\
\dfrac{\mathrm{d}^2V_{p_1}(t)}{\mathrm{d}t^2} = \alpha\beta(v_{\mathrm{stim}}S(t_{\mathrm{s}})) - (\alpha+\beta)\dot{V}_{p_1}(t),\\
\dfrac{\mathrm{d}^2V_r(t)}{\mathrm{d}t^2} = \alpha\beta(-V_r(t) + v_{re}\phi_e(t) + v_{rp_1}S(V_{p_1}(t)) + v_{rs}S(V_s(t))) - (\alpha+\beta)\dot{V}_r(t),\\
\dfrac{\mathrm{d}^2V_s(t)}{\mathrm{d}t^2} = \alpha\beta(-V_s(t) + v_{se}\phi_e(t) + v_{sp_1}S(V_{p_1}(t)) + v_{sr}^AS(V_r(t))\\
\qquad\qquad + v_{sr}^BS(V_r(t-\tau)) + \phi_n) - (\alpha+\beta)\dot{V}_s(t),
\end{cases} \tag{8}$$

where the external stimulus ($t_{\rm s}$) is applied to GPI handled by the sigmoid function S and multiplied by the stimulation strength parameters $v_{\rm stim}$, which is the only input of GPI, and the details of the TPDS are described in the next subsection.

2.2 Tri-phase delay stimulus setup

Inspired by the electrophysiological observation that there exist significantly different information transmission delays for the direct, indirect, and hyperdirect pathways to GPI[40–41,43], we propose a new tri-phase delay stimulation (TPDS, shown in Fig. 1(c)), which successively applies tri-phase pulses in each period of TPDS to GPI representing the inputs from D_1, GPE, and STN, respectively, with the pulse gap comparative to the transmission delays. In particular, because the transmission delay of STN-GPI is the smallest, and the function of STN on GPI is excitatory, the first phase in each period of TPDS is positive (anodic phase). Similarly, the next two cathodic phases represent the inhibitory functions of the D_1-GPI and GPE-GPI pathways. Stimulation amplitudes are denoted by A_1, A_2, and A_3, respectively. W is the pulse width, and f is the stimulation frequency. TPDS can be modeled as

$$t_{\rm s}=\begin{cases}A_1, & t\in(k\tau_1,k(\tau_1+W)),\\ A_2, & t\in(k(\tau_1+\tau_2+W),k(\tau_1+\tau_2+2W)),\\ A_3, & t\in(k(\tau_1+\tau_2+\tau_3+2W),k(\tau_1+\tau_2+\tau_3+3W)),\\ 0, & \text{others},\end{cases} \tag{9}$$

and

$$\phi_{\rm stim}=v_{\rm stim}S(t_{\rm s}), \tag{10}$$

where $k=1,2,3,\cdots$, and τ_1, τ_2, and τ_3 are the three time delays, based on which the information transmission delays of the hyperdirect, direct and indirect pathways of basal ganglia can be deduced as $\tau_1:(\tau_1+\tau_2):(\tau_1+\tau_2+\tau_3)$. The input signal to the GPI can be acquired by the weighted sigmoid function transferring the time series of the stimulus into the stimulation rate change over time. And the parameter $v_{\rm stim}$ is the parameter representative of the strength of the total stimulus from the electrode, which is set at about 0.8 mV $\cdot$ s.

2.3 Model parameters

The parameters used in the simulation of the original model and GCT model are listed in Table 1, which are mainly acquired from the previous researches and models[16, 18, 19, 38, 41–43, 47, 48]. The parameters of TPDS are given in Table 2, where the time delays between pulses (i.e., pulse gap) in TPDS during the calculation are set as 4.74 ms, 8.5 ms, and 4.75 ms according to the ratio of about 1:2:1. Hence the ratio of transmission delays is 1:3:4, which is consistent with the experimental observation.

3 Results

3.1 Triple adjustment of D_1-GPI, GPE-GPI, STN-GPI for absence seizures

Since the three-phase pulses with pulse gap of TPDS mainly represent the functions of three input pathways on GPI, the triple adjustment of D_1-GPI, GPE-GPI, and STN-GPI based on the BGCT model should be firstly investigated to verify the effect of TPDS on the seizure regulation.

To clearly observe the effect of the triple adjustment of D_1-GPI, GPE-GPI, and STN-GPI, Figs. 2(c) and 2(d) give the state bifurcation and corresponding dominant frequency on the two-dimensional (2D) plane of v_{se} and τ based on the original BGCT model in the presence of functions of D_1, GPE, and STN. As shown in Fig. 2(c), four different states are displayed where state 1 is the low firing state (blue, Fig. 2(e)), state 2 is the simple oscillation state (cyan, Fig. 2(f)), state 3 is the classical hallmark of absence seizure, i.e., the SWDs state (yellow, Fig. 2(g)) of 2 Hz–4 Hz, and state 4 is the saturation state (brown, Fig. 2(h)). It can be seen that for the lower and larger v_{se}, and the system lies in the non-seizure states, showing low and

Table 1 Default parameters for BGCT model

Symbol	Value	Description	Reference
$Q_e^{\max}, Q_i^{\max}$	250 Hz	Cortex neurons' maximum firing rate	[16,18,19,38,42]
$Q_{d1}^{\max}, Q_{d2}^{\max}$	65 Hz	Striatum neurons' maximum firing rate	[18,19,36,37]
$Q_{p1}^{\max}$	250 Hz	SNr neurons' maximum firing rate	[18,19,36,37]
$Q_{p2}^{\max}$	300 Hz	GPE neurons' maximum firing rate	[18,19,36,37]
$Q_{\zeta}^{\max}$	500 Hz	STN neurons' maximum firing rate	[18,19,36,37]
$Q_s^{\max}$	250 Hz	SRN neurons' maximum firing rate	[16,18,19,38,42]
$Q_r^{\max}$	250 Hz	TRN neurons' maximum firing rate	[16,18,19,38,42]
θ_e, θ_i	15 mV	Mean firing threshold of cortex neurons	[16,18,19,38,42,43]
θ_{d1}, θ_{d2}	19 mV	Mean firing threshold of striatum neurons	[18,19,36,37]
θ_{p1}	10 mV	Mean firing threshold of SNr neurons	[18,19,36,37]
θ_{p2}	9 mV	Mean firing threshold of GPE neurons	[18,19,36,37]
θ_{ζ}	10 mV	Mean firing threshold of STN neurons	[18,19,36,37]
θ_s	15 mV	Mean firing threshold of SRN neurons	[16,18,19,38,42,43]
θ_r	15 mV	Mean firing threshold of TRN neurons	[16,18,19,38,42,43]
v_{ee}	1 mV · s	Couping strength among excitatory pyramidal neurons	[16,18,19,42]
$-v_{ei}$	1.8 mV · s	Couping strength from IIN to EPN	[16,18,19,42]
v_{re}	0.05 mV · s	Couping strength from EPN to TRN	[18,19,38,42]
v_{rs}	0.5 mV · s	Couping strength from SRN to TRN	[18,19,38,42]
$-v_{sr}^{A,B}$	0.4 mV · s–2 mV · s	Couping strength from TRN to SRN	[18,19,38,43]
v_{d1e}	1 mV · s	Couping strength from EPN to striatal D_1 neurons	[18,19,36,37]
$-v_{d1d1}$	0.2 mV · s	Couping strength among striatal D_1 neurons	[18,19,36,37]
v_{d1s}	0.1 mV · s	Couping strength from SRN to striatal D_1 neurons	[18,19,36,37]
v_{d2e}	0.7 mV · s	Couping strength from EPN to striatal D_2 neurons	[18,19,36,37]
$-v_{d2d2}$	0.3 mV · s	Couping strength among striatal D_2 neurons	[18,19,36,37]
v_{d2s}	0.05 mV · s	Couping strength from SRN to striatal D_2 neurons	[18,19,36,37]
$-v_{p1d1}$	0.1 mV · s	Couping strength from striatal D_1 neurons to SNr	[18,19,36,37]
$-v_{p1p2}$	0.03 mV · s	Couping strength from GPE to SNr	[18,19,36,37]
$v_{p1\zeta}$	0 mV · s–0.6 mV · s	Couping strength from STN to SNr	[18,19,36,37]
$-v_{p2d2}$	0.3 mV · s	Couping strength from striatal D_2 neurons to GPE	[18,19,36,37]
$-v_{p2p2}$	0.0075 mV · s	Couping strength among GPE neurons	[18,19,36,37]
$v_{p2\zeta}$	0.45 mV · s	Couping strength from STN to GPE	[18,19,36,37]
$-v_{\zeta p2}$	0.04 mV · s	Couping strength from GPE to STN	[18,19,36,37]
v_{es}	1.8 mV · s	Couping strength from SRN to EPN	[18,19,39,42]
v_{se}	2.2 mV · s	Couping strength from EPN to SRN	[18,19,39]
$v_{\zeta e}$	0.1 mV · s	Couping strength from EPN to STN	[18,19,36,37]
$-v_{sp1}$	0.035 mV · s	Couping strength from GPI neurons to SRN	[18,19,36,37]
$-v_{rp1}$	0.035 mV · s	Couping strength from GPI neurons to TRN	[18,19]
γ_e	100 Hz	Cortical damping rate	[16,18,19,38,42]
τ	50 ms	Time delay due to slow synaptic kinetics of GABAb	[18,19,42]
α	50 s^{-1}	Synaptodendritic decay time constant	[16,18,19,38,42,43]
β	200 s^{-1}	Synaptodendritic rise time constant	[16,18,19,38,42,43]
σ	6 mV	Threshold variability of firing rate	[16,18,19,38,43]
ϕ_n	2 mV · s	General subthalamic input onto SRN	[16,18,19,38,43]

Table 2 Default parameters for TPDS

Symbol	Value	Description	Reference
A	10 mV	Amplitudes of stimulus	Estimated
f	50 Hz	Frequency of stimulus	Estimated
W	1 ms	Width of impulses of stimulus	Estimated
τ_1	4.74 ms	Time delay before first phase of TPDS in a period	[33]
τ_2	8.5 ms	Time delay before second phase of TPDS in a period	[33]
τ_3	4.75 ms	Time delay before third phase of TPDS in a period	[33]
v_{stim}	0.8 mV · s	Strength of TPDS applied to GPI	Estimated

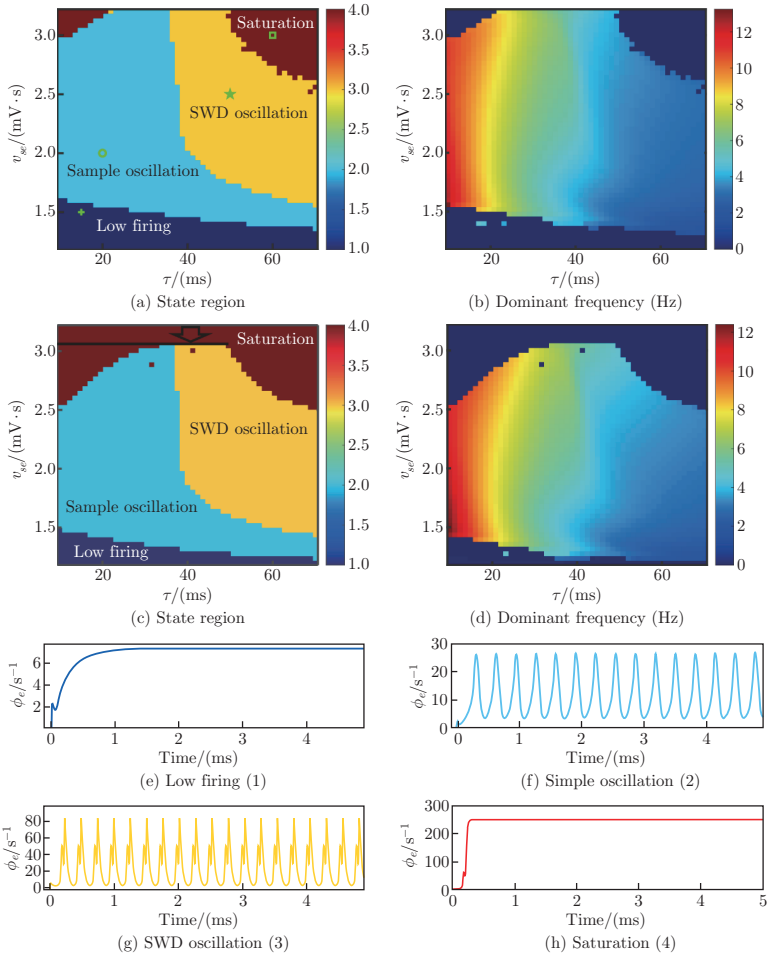

Fig. 2 (a) Two-parameter dynamic state diagram of v_{se} (connection strength from excitatory cortical pyramidal neurons to SRN) and τ (time delay of GABAb connection) parameters in absence of inputs from GPE, STNs, and striatum D_1 populations ($v_{p1p2} = v_{p1\zeta} = v_{p1d1} = 0$). (b) Two-dimension frequency analysis in (v_{se}, τ) panel corresponding to conditions of (a). (c) Two-parameter dynamic state diagram of v_{se} and τ with inputs from GPE, STN, and striatum D_1 populations ($v_{p1\zeta} = 0.3\ \mathrm{mV}\cdot\mathrm{s}$, $v_{p1d1} = 0.1\ \mathrm{mV}\cdot\mathrm{s}$, $v_{p1p2} = 0.03\ \mathrm{mV}\cdot\mathrm{s}$). (d) Two-dimension frequency analysis in (v_{se}, τ) panel corresponding to conditions of (c). Four types of dynamical state regions are given in (a) and (c), which are low firing rate region (1), simple oscillation region (2), SWD oscillation region (3), and saturation region (4), and different typical time series of four dynamical states are shown in (e)–(h), which are corresponding to points in (a) (low firing: $v_{se} = 1.5\ \mathrm{mV}\cdot\mathrm{s}$, $\tau = 15\,\mathrm{ms}$, green cross; sample oscillation: $v_{se} = 2\ \mathrm{mV}\cdot\mathrm{s}$, $\tau = 20\ \mathrm{ms}$, green circle; SWD Oscillation: $v_{se} = 2.5\ \mathrm{mV}\cdot\mathrm{s}$, $\tau = 50\,\mathrm{ms}$, green five-pointed star; saturation: $v_{se} = 3\ \mathrm{mV}\cdot\mathrm{s}$, $\tau = 60\ \mathrm{ms}$, green square) (color online)

saturated firings, respectively. This corresponds to the weak and strong recurrent excitations between cortex and SRN, and the GABAb-mediated connection delay τ from TRN and SRN seems not to work on them. But for the moderate v_{se}, lower delay τ makes the system show simple oscillations, while the larger delay τ can induce the 2 Hz–4 Hz SWD discharges of the system. This state transition with the increasing of τ is mainly determined by the GABAa (fast dynamics) and GABAb (slow dynamics) mediated dual actions of TRN. In the case of lower delay, the dual action of GABAa and GABAb can nearly simultaneously function, the system shows simple oscillation with the spikes of the same amplitude. But in the case of a larger

delay, the GABAergic actions between GABAa and GABAb have a delay τ, that is, τ ms later after the GABAergic actions of GABAa, GABAb begins to join into the GABAergic actions on SRN, which ultimately results in the SWD discharges with spikes of having two different amplitudes. In addition, it is noted that the SWD control can be performed in more than three directions including vertically upwards and downwards as well as horizontally leftwards.

Next, compared with Fig. 2(c), in the absence of the inputs from D_1, GPE, and STN, i.e., all the D_1-GPI, GPE-GPI, and STN-GPI pathways are blocked, Fig. 2(a) shows that the seizure pattern on the plane of (v_{se}, τ) is moved up in total which leads to the larger parameter region corresponding to low firings while the parameter region corresponding to saturated states is significantly decreased. This suggests the D_1-GPI, GPE-GPI, and STN-GPI pathways indeed play roles in affecting GPI-regulated seizure patterns. However, at this time, the SWD can mainly be controlled by only the vertical downward and horizontal leftward directions.

To investigate the independent effect of each pathway, we separately block the three inputs into GPI, i.e., every time we block one pathway and observe the effect of the other pathways on seizure patterns. In Fig. 3, we block (i.e., setting the coupling strength is 0) the STN-GPI (Fig. 3(a)), D_1-GPI (Fig. 3(b)) and GPE-GPI (Fig. 3(c)), respectively. By comparing Fig. 3 with Fig. 2(c), it can be seen that STN has the opposite functions to D_1 and GPE for the occurrence of saturated states. In particular, STN is in favor of the generation of a saturated state, but D_1 and GPE are unfavorable for the generation of saturated state. This is because STN first excites GPI, then GPI more strongly inhibits TRN which lastly activates the recurrent excitation between SRN and cortex by disinhibiting SRN, leading to the saturated state. In contrast, both D_1 and GPE first inhibit GPI, GPI then disinhibits TRN which weakens the recurrent excitation between SRN and cortex by more strongly inhibiting SRN, leading to the

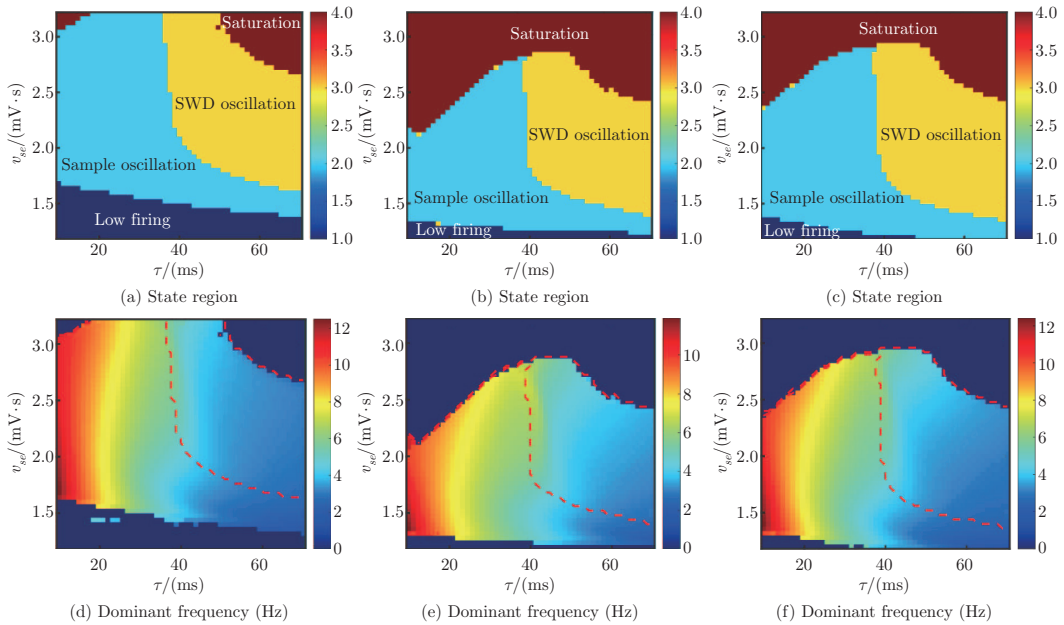

Fig. 3 (a) State bifurcations on 2D plane composed of v_{se} and τ in absence of inputs from STN ($v_{p1\zeta} = 0$, $v_{p1d1} = 0.1$ mV·s, $v_{p1p2} = 0.03$ mV·s). (b) State bifurcations on 2D plane composed of v_{se} and τ in absence of inputs from striatum D_1 ($v_{p1d1} = 0$, $v_{p1\zeta} = 0.3$ mV·s, $v_{p1p2} = 0.03$ mV·s). (c) State bifurcations on the 2D plane composed of v_{se} and τ in absence of inputs from GPE ($v_{p1p2} = 0$, $v_{p1\zeta} = 0.3$ mV·s, $v_{p1d1} = 0.1$ mV·s). (d), (e), and (f) are corresponding frequency analysis diagrams of (a)–(c) and dominant frequency range of SWDs state has been circled by red dotted line in (d)–(f). By comparison of state distribution of diagrams (a)–(c), effect of modulation from STN is the most prominent (color online)

occurrences of simple oscillations or SWD discharges.

To schematically observe the triple effects of the STN-GPI, D_1-GPI, and GPE-GPI, Figs. 4(a) and 4(c) give the state bifurcations on the 2D planes of ($v_{p1\zeta}$,v_{p1d1}) and ($v_{p1\zeta}$,v_{p1p2}), with fixing v_{p1p2}=0.03 mV · s and v_{p1d1}=0.1 mV · s, respectively. Figures 4(b) and 4(d) are the corresponding dominant frequencies. It is clearly observed from Figs. 4(a) and 4(b) that by strengthening the excitation from STN to GPI, i.e., by increasing the $v_{p1\zeta}$, SWD discharges can be effectively controlled and the system transitions into the saturation state. In addition, for the moderate $v_{p1\zeta}$, the system can also transition from the SWD to saturation by decreasing v_{p1d1}, i.e., the inhibition from D_1 to p_1. Similar schematic for the combined effect of STN and GPE on the plane of ($v_{p1\zeta}$,v_{p1p2}) can be seen in Figs. 4(c) and 4(d).

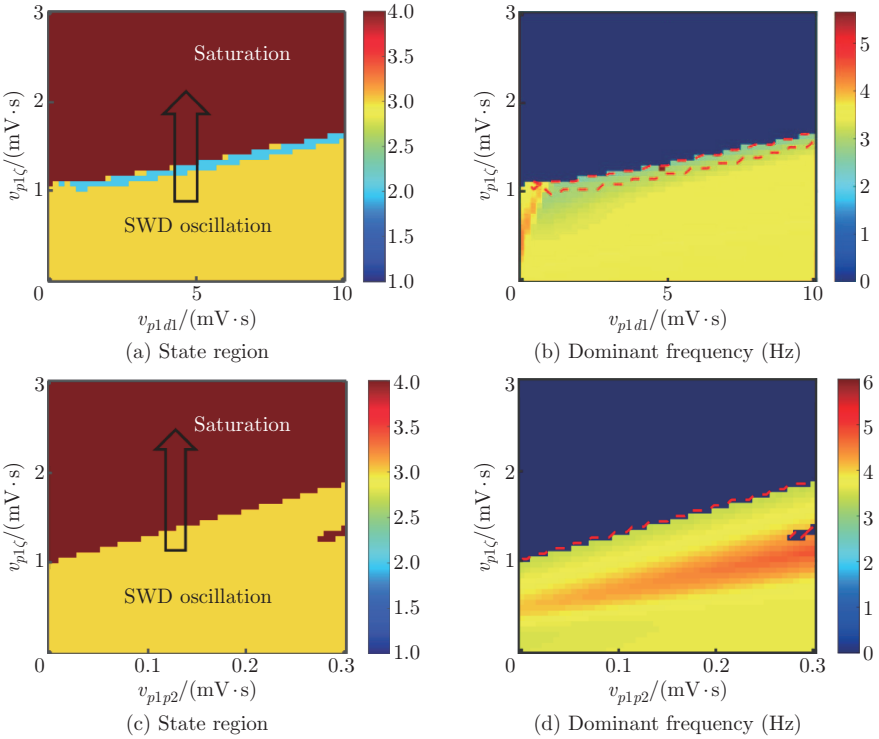

(a) State region (b) Dominant frequency (Hz)

(c) State region (d) Dominant frequency (Hz)

Fig. 4 (a) State bifurcations on 2D plane composed of $v_{p1\zeta}$ and v_{p1d1} of BGCT model ($v_{p1p2} = 0.03$ mV · s). (b) $v_{p1\zeta}$ corresponds dominant frequency analysis of (a). (c) State bifurcations on 2D plane composed of $v_{p1\zeta}$ and v_{p1p2} ($v_{p1d1} = 0.1$ mV · s). (d) v_{p1d1} corresponds dominant frequency analysis of (c). Bottom areas below red dotted lines in (b) and (d) are areas of dominant frequency corresponding to SWDs state. v_{se} is 2.2 mV · s, and time delay of GABAb τ is 50 ms. Besides, cyan area is area of simple oscillation (2), yellow area is area of SWD oscillation (3), and red area corresponds to saturation state (4) (color online)

In conclusion, by the simulation of the BGCT model, the regulation mechanisms of the three input populations to GPI have been preliminarily researched. Results show that all the STN, D_1, and GPE can control the dynamic states of the whole system by changing the activity of the GPI. These results provide suggestions for the parameters optimization of the TPDS which will be used in the following sections to simulate the substitution effect of STN-GPI, D_1-GPI, and GPE-GPI pathways based on the reduced GCT model.

3.2 Surrogate function of tri-phase delay stimulation for GPE-GPI, STN-GPI, D_1-GPI

The external stimulus has been evidenced to act as a measure of stopping the seizures by taking the role of regulating the internal circuit dynamic behaviors. To investigate the substitute

function of TPDS in performing the seizure pattern modulation of basal ganglia when the GPE-GPI, STN-GPI, and D_1-GPI pathways are blocked, in this section, the calculations are conducted based on the reduced GCT model. Figures 5(a) and 5(b) give the state bifurcation and dominant frequency distribution on the plane of (v_{se},τ) based on the GCT model, which, in essence, is same as the result calculated based on the BGCT model as shown in Fig. 2(a).

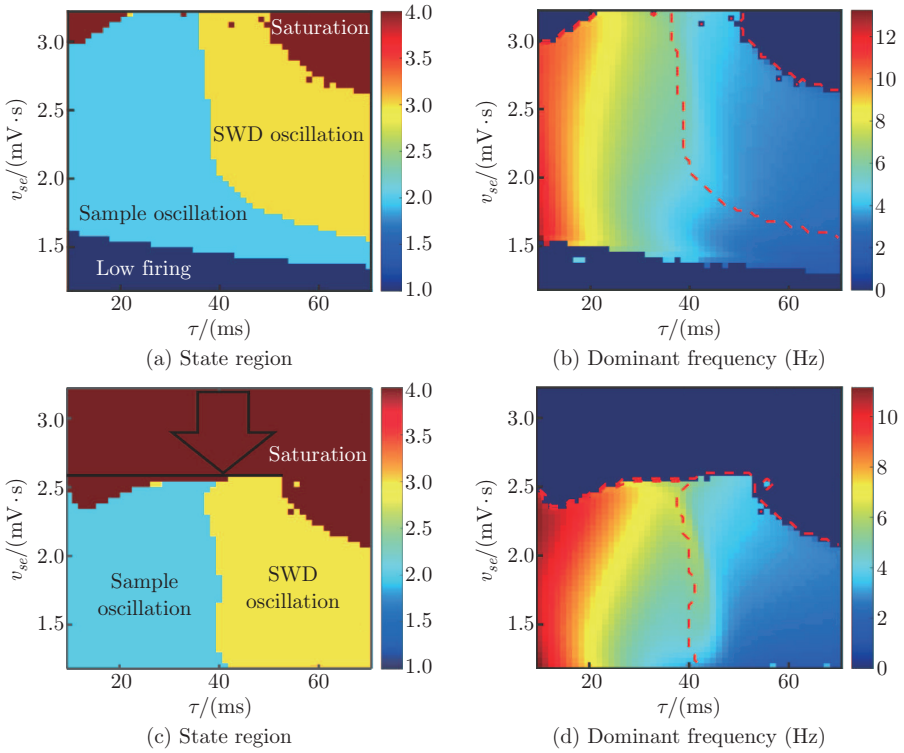

Fig. 5 State bifurcations on 2D plane composed of v_{se} and τ of GCT model in absence and presence of external stimulus, with fixing $v_{\text{stim}} = 0$ (a) and $v_{\text{stim}} = 0.8$ mV·s (c), respectively. (b) and (d) are corresponding dominant frequency analysis of (a) and (c), and areas between red dotted lines are dominant frequencies corresponding to 2 Hz–4 Hz SWD discharges. Here, stimulation amplitudes of TPDS are uniformly set as 10 mV, pulse width W is 1 ms, and frequency used here is 50 Hz (color online)

Then, we apply TPDS to GPI to observe the modulating effect on the seizure pattern. As shown in Fig. 2, the seizure pattern of the system with the inputs from GPE, STN, and D_1 to GPI is moved down on the whole compared to the case without the three inputs into GPI. Interestingly, as shown in Fig. 5(c), the whole seizure pattern can also be moved down (indicated by the arrow) by performing the TPDS instead of the three inputs into GPI. The similarity between the internal control by the inputs from STN, striatum D_1 and GPE and external control of TPDS is computationally found. This suggests that TPDS can indeed play the surrogate modulation role similar to basal ganglia, which might be helpful for the development of the brain-computer interface in the clinical application of epilepsy.

3.3 Control effect on absence seizures

In addition, it is also important to further control or abate seizures by well-tuning the TPDS stimulation parameters, which is the key factor for the application of the brain-computer interface in clinical epilepsy. In order to determine the optimized parameter for effectively controlling seizure, as an illustration, the system is initially set as SWD discharges which correspond to the parameter point (v_{se}, τ)=(2.2 mV·s, 50 ms) in Fig. 5(a), and then to observe

the abatement effect of TPDS by changing the stimulation amplitudes, stimulation frequency, and pulse width.

Figure 6 shows the seizure control effect with changing stimulation amplitudes of the three-phase pulse of TPDS. Here, A_1, A_2, and A_3 are the anodic (A_1) and cathodic (A_2, A_3) phase pulse amplitudes corresponding to the input strengths from STN, D_1, and GPE, respectively. In Fig. 6(a), we provide the seizure type transitions on the planes of (A_1, A_2) with fixing $A_3 = 10$ mV. It is clearly seen that increasing the anodic phase pulse amplitude (A_1) can effectively drive the system from SWD discharges into saturated states, leading to the seizure termination. By contrast, the cathodic phase pulses (A_2, A_3) have little influence on the seizure termination. A Similar schematic can be found in Fig. 6(c). This result is unsurprising but interestingly consistent with the findings from Fig. 3 and Fig. 4 that the excitatory inputs to GPI from STN play a more dominant role in the formation of seizure patterns.

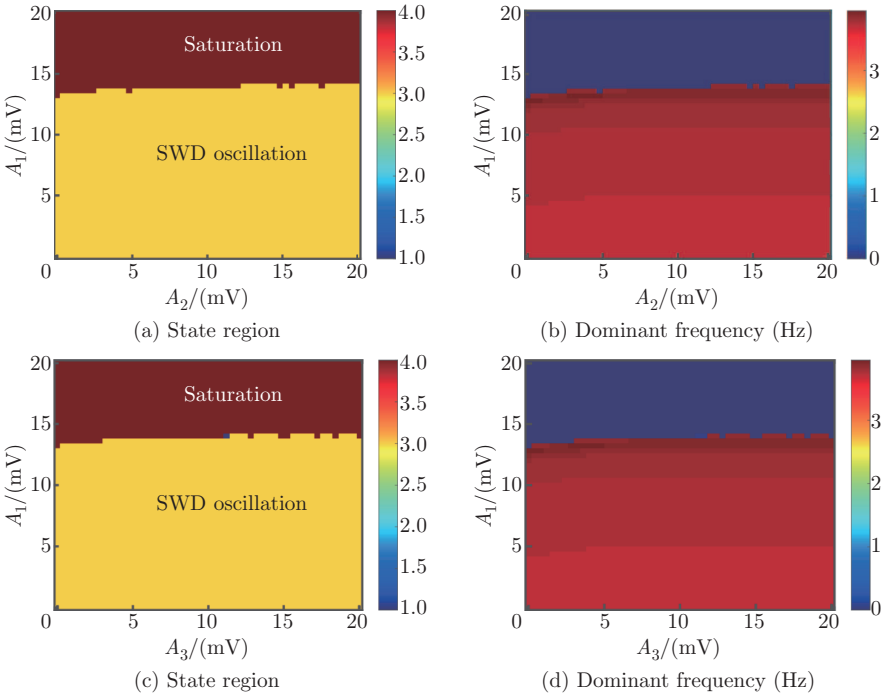

Fig. 6 (a) State bifurcations on 2D plane composed of phase amplitudes A_1 and A_2 of TPDS with fixing phase amplitude $A_3 = 10$ mV. (b) Dominant frequency analysis diagrams of (a). (c) State bifurcations on 2D plane composed of phase amplitudes A_1 and A_3 of TPDS with fixing phase amplitude $A_2 = 10$ mV. (d) Dominant frequency analysis diagrams of (c). Other parameters are kept of default values (see Tables 1 and 2), stimulus frequency $f = 50$ Hz, pulse width $W = 1$ ms, and stimulus strength $v_{\text{stim}} = 0.8$ mV·s. And coupling strength $v_{se} = 2.2$ mV·s, time delay of GABAb $\tau = 50$ ms corresponding to points in SWDs state of Fig. 5(a) (color online)

Besides the amplitudes of different phases of TPDS, the control effects of the external stimulus are also proven to have something to do with the stimulation frequency and pulse width[28–30]. For simplicity, we here suppose the amplitudes of the three-phase pulses of TPDS are changing synchronously, and then investigate the combined effect of stimulation amplitude with stimulation frequency (f) and pulse width (W), respectively. The results of the state region transition and dominant frequency distribution on the plane of (A, f) and (A, W) are exhibited in Figs. 7(a), 7(b), Figs. 7(c), and 7(d), respectively.

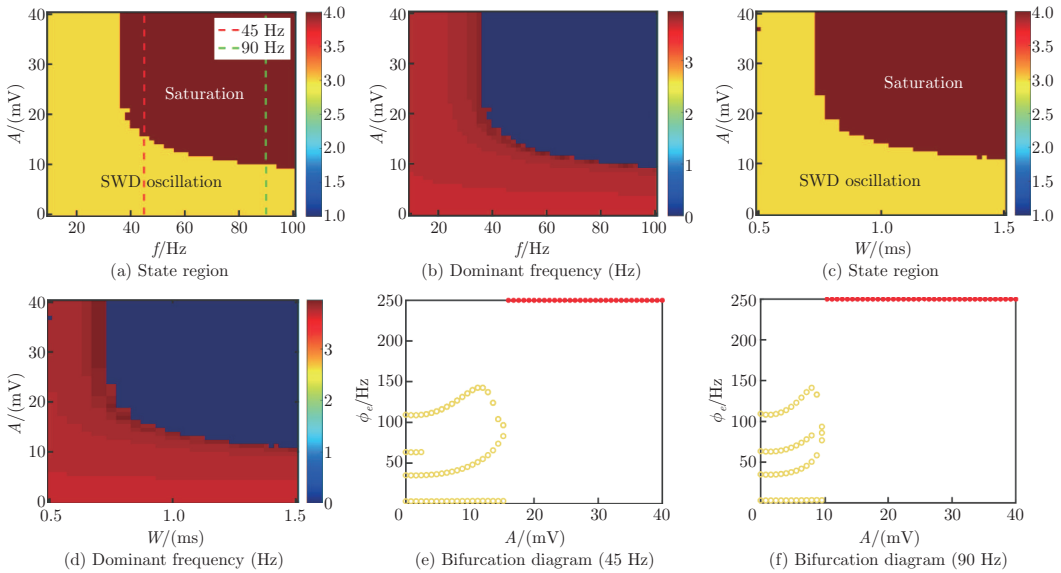

(a) State region (b) Dominant frequency (Hz) (c) State region

(d) Dominant frequency (Hz) (e) Bifurcation diagram (45 Hz) (f) Bifurcation diagram (90 Hz)

Fig. 7 (a) State bifurcations on 2D plane composed of stimulation amplitude A and stimulation frequency f with pulse width $W = 1$ ms. (c) State bifurcations on 2D plane composed of stimulation amplitude A and pulse width W with frequency $f = 50$ Hz. (b) and (d) are dominant frequency analysis diagrams of (a) and (c). (e) and (f) are bifurcation diagrams of ϕ_e with respect to stimulation amplitude with fixing stimulation frequency $f = 45$ Hz and $f = 90$ Hz (marked in (a) in red and green dotted line), respectively. Here $A = A_1 = A_2 = A_3$, and the stimulus strength $v_{\text{stim}} = 0.8$ mV · s; Coupling strength $v_{se} = 2.2$ mV · s, and time delay of GABAb $\tau = 50$ Hz, which corresponds to SWDs state in Fig. 5(a) (color online)

It is seen from Fig. 7 that only for specific stimulation frequency and pulse width, stimulation can effectively abate seizures. With further increase in the stimulation frequency and pulse width, the amplitude of stimulation can take effect in controlling seizures decreases. This can be clearly observed in Figs. 7(e) and 7(f) where we give the cases of $f = 45$ Hz (Fig. 7(e)) and $f = 90$ Hz (Fig. 7(f)), respectively. Similarly, only for the specific stimulation amplitude, stimulation can effectively abate seizures, where with further increase of the stimulation amplitude, the corresponding stimulation frequency, and pulse width can take effect in controlling seizure decreases. In particular, for the large enough stimulation amplitude, frequency, and pulse width, SWD can be robustly abated in the relatively large parameter regions.

4 Conclusions

In sum, based on the modulation of basal ganglia for the absence seizures, the three-pathway structure of basal ganglia composed of direct, indirect, and hyperdirect pathways, as well as the electrophysiological observation that there exist significantly different information transmission delays for the three pathways, we develop a reduced GCT model and computationally proposed a new TPDS. Because these three pathways are converged into the main output nucleus of basal ganglia, the GPI, from the striatal D_1 neurons, STN, and GPE, respectively, based on the BGCT model, we first investigate the control effect of the D_1-GPI, GPE-GPI, and STN-GPI pathways on seizures by regulating the activity of GPI.

Then, based on the GCT model, we use the TPDS on GPI to investigate the reproducing effects for the seizure pattern and the abating effect for seizure activity. This is to find and verify the alternative and improved approaches for the dysregulation of basal ganglia. Here, dysregulation means the D_1-GPI, GPE-GPI, and STN-GPI pathways are blocked or broken.

It is computationally testified that TPDS can effectively reproduce the seizure pattern and further abate seizures by well-tuning TPDS parameters. Perhaps, TPDS is not the strongest form of electrical stimulation to control seizures acting on GPI, but the stimulation form of TPDS conforms to the rule of internal stimulation, which has physiological rationality and potential for further development. At the same time, TPDS can also produce less damage in the form of alternating electrode stimulation compared with some traditional stimulation forms, which is helpful to reduce postoperative sequelae. Hopefully, the design idea of TPDS can also enlighten the form design referring to the form of endogenous regulation of stimulus of different targets. The final results suggest that TPDS can play the surrogate modulation role similar to basal ganglia which might be helpful for the development of the brain-computer interface in the clinical application of epilepsy.

5 Author contributions

All authors designed and performed the research, and analyzed the data as well as wrote the paper.

References

[1] PANAYIOTOPOULOS, C. P. Typical absence seizures and their treatment. *Archives of Disease in Childhood*, **81**(4), 351–355 (1999)

[2] MOSHÉ, S. L., PERUCCA, E., RYVLIN, P., and TOMSON, T. Epilepsy: new advances. *The Lancet*, **385**(9971), 884–898 (2015)

[3] DURÓN, R. M., MEDINA, M. T., MARTÍNEZ-JUÁREZ, I, E., BAILEY, J. N., PEREZ-GOSIENGFIAO, K. T., RAMOS-RAMÍREZ, R., LÓPEZ-RUIZ, M., ALONSO, M. E., ORTEGA, R. H., PASCUAL-CASTROVIEJO, I., MACHADO-SALAS, J., MIJA, L., and DELGADO-ESCUETA, A. V. Seizures of idiopathic generalized epilepsies. *Epilepsia*, **46**(s9), 34–47 (2005)

[4] VOLMAN, V., PERC, M., and BAZHENOV, M. Gap junctions and epileptic seizures-two sides of the same coin? *PLoS One*, **6**(5), e20572 (2011)

[5] JASPER, H. and KERSHMAN, J. Electroencephalographic classification of the epilepsies. *Archives of Neurology and Psychiatry*, **45**(6), 903–943 (1941)

[6] LÜTTJOHANN, A. and VAN LUIJTELAAR, G. Thalamic stimulation in absence epilepsy. *Epilepsy Research*, **106**(1), 136–145 (2013)

[7] LÜTTJOHANN, A., SCHOFFELEN, J. M., and VAN LUIJTELAAR, G. Termination of ongoing spike-wave discharges investigated by cortico-thalamic network analyses. *Neurobiology of Disease*, **70**, 127–137 (2014)

[8] PAZ, J. T., DAVIDSON, T. J., FRECHETTE, E. S., DELORD, B., PARADA, I., PENG, K., DEISSEROTH, K., and HUGUENARD, J. R. Closed-loop optogenetic control of thalamus as a tool for interrupting seizures after cortical injury. *Nature Neuroscience*, **16**(1), 64–70 (2013)

[9] MARESCAUX, C. and VERGNES, M. Genetic absence epilepsy in rats from strasbourg (GAERS). *Italian Journal of Neurological Sciences*, **16**(1), 113–118 (1995)

[10] COENEN, A. M. L. and VAN LUIJTELAAR, E. L. J. M. Genetic animal models for absence epilepsy: a review of the WAG/Rij strain of rats. *Behavior Genetics*, **33**(6), 635–655 (2003)

[11] TIMOFEEV, I. and STERIADE, M. Neocortical seizures: initiation, development and cessation. *Neuroscience*, **123**(2), 299–336 (2004)

[12] LYTTON, W. W. Computer modelling of epilepsy. *Nature Reviews Neuroscience*, **9**(8), 626–637 (2008)

[13] DESTEXHE, A. Spike-and-wave oscillations based on the properties of GABAb receptors. *Journal of Neuroscience the Official Journal of the Society for Neuroscience*, **18**(21), 9099–9111 (1998)

[14] DESTEXHE, A. Can GABAa conductances explain the fast oscillation frequency of absence seizures in rodents? *European Journal of Neuroscience*, **11**(6), 2175–2181 (1999)

[15] SUFFCZYNSKI, P., KALITZIN, S., and DA SILVA, F. H. Dynamics of non-convulsive epileptic phenomena modeled by a bistable neuronal network. *Neuroscience*, **126**(2), 467–484 (2004)

[16] BREAKSPEAR, M., ROBERTS, J. A., TERRY, J. R., RODRIGUES, S., MAHANT, N., ROBINSON, P. A. A unifying explanation of primary generalized seizures through nonlinear brain modeling and bifurcation analysis. *Cerebral Cortex*, **16**(9), 1296–1313 (2006)

[17] DA SILVA, F. L., BLANES, W., KALITZIN, S. N., PARRA, J., SUFFCZYNSKI, P., and VELIS, D. N. Epilepsies as dynamical diseases of brain systems: basic models of the transition between normal and epileptic activity. *Epilepsia*, **44**(s12), 72–83 (2003)

[18] CHEN, M. M., GUO, D. Q., WANG, T. B., JING, W., and XIA, Y. Bidirectional control of absence seizures by the basal ganglia: a computational evidence. *PLoS Computational Biology*, **10**(3), e1003495 (2014)

[19] CHEN, M. M., GUO, D. Q., LI, M., MA, T., WU, S. D., YAN, J. J., and XIA, Y. Critical roles of the direct gabaergic pallido-cortical pathway in controlling absence seizures. *PLoS Computational Biology*, **11**(10), e1004539 (2015)

[20] DERANSART, C., VERCUEIL, L., MARESCAUX, C., and DEPAULIS, A. The role of basal ganglia in the control of generalized absence seizures. *Epilepsy Research*, **32**(1), 213–223 (1998)

[21] LUO, C., LI, Q., XIA, Y., LEI, X., XUE, K., YANG, Z., MARTÍNEZ-MONTES, E., LIAO, W., and ZHOU, D. Resting state basal ganglia network in idiopathic generalized epilepsy. *Human Brain Mapping*, **33**(6), 1279–1294 (2012)

[22] PAZ, J. T., CHAVEZ, M., SAILLET, S., DENIAU, J. M., and CHARPIER, S. Activity of ventral medial thalamic neurons during absence seizures and modulation of cortical paroxysms by the nigrothalamic pathway. *Journal of Neuroscience the Official Journal of the Society for Neuroscience*, **27**(4), 929–941 (2007)

[23] MANNING, J. P. A., RICHARDS, D. A., and BOWERY, N. G. Pharmacology of absence epilepsy. *Trends in Pharmacological Sciences*, **24**(10), 542–549 (2003)

[24] MASUR, D., SHINNAR, S., CNAAN, A., SHINNAR, R. C., and GLAUSER, T. A. Pretreatment cognitive deficits and treatment effects on attention in childhood absence epilepsy. *Neurology*, **81**(18), 1572–1580 (2013)

[25] RUSSO, E., CITRARO, R., SCICCHITANO, F., DE FAZIO, S., PAOLA, E. D. D., CONSTANTI, A., and DE SARRO, G. Comparison of the antiepileptogenic effects of an early long-term treatment with ethosuximide or levetiracetam in a genetic animal model of absence epilepsy. *Epilepsia*, **51**(8), 1560–1569 (2010)

[26] KWAN, P., ARZIMANOGLOU, A., BERG, A. T., BRODIE, M. J., HAUSER, A., MATHERN, G., MOSHÉ, S. L., PERUCCA, E., WIEBE, S., and FRENCH, J. Definition of drug resistant epilepsy: consensus proposal by the ad hoc task force of the ilae commission on therapeutic strategies. *Epilepsia*, **51**(6), 1069–1077 (2010)

[27] BENABID, A. L., CHABARDES, S., MITROFANIS, J., and POLLAK, P. Deep brain stimulation of the subthalamic nucleus for the treatment of Parkinson's disease. *The Lancet Neurology*, **8**(1), 67–81 (2009)

[28] KILE, K. B., TIAN, N., and DURAND, D. M. Low frequency stimulation decreases seizure activity in a mutation model of epilepsy. *Epilepsia*, **51**(9), 1745–1753 (2010)

[29] BIKSON, M. Suppression of epileptiform activity by high frequency sinusoidal fields in rat hippocampal slices. *Journal of Physiology*, **531**(1), 181–191 (2001)

[30] CHIANG, C. C., LIN, C. C. K., JU, M. S., and DURAND, D. M. High frequency stimulation can suppress globally seizures induced by 4-AP in the rat hippocampus: an acute in vivo study. *Brain Stimulation*, **6**(2), 180–189 (2013)

[31] FAN, D., ZHENG, Y., YANG, Z., and WANG, Q. Improving control effects of absence seizures using single-pulse alternately resetting stimulation (SARS) of corticothalamic circuit. *Applied Mathematics and Mechanics* (*English Edition*), **41**(9), 1287–1302 (2020) https://doi.org/10.1007/s10483-020-2644-8

[32] YU, Y., WANG, X., WANG, Q., and WANG, Q. A review of computational modeling and deep brain stimulation: applications to Parkinson's disease. *Applied Mathematics and Mechanics* (*English Edition*), **41**(12), 1747–1768 (2020) https://doi.org/10.1007/s10483-020-2689-9

[33] HAGHIGHI, H. S. and MARKAZI, A. H. D. Control of epileptic seizures by electrical stimulation: a model-based study. *Biomedical Physics and Engineering Express*, **7**(6), 065009 (2021)

[34] BORDEY, A. Treating seizures with low-frequency electrical stimulation. *Epilepsy Currents*, **21**(3), 197–198 (2021)

[35] ZHANG, H., ZHAO, Y., SHEN, Z., CHEN, F., CAO, Z., and SHAN, W. Control analysis of optogenetics and deep brain stimulation targeting basal ganglia for Parkinson's disease. *Era*, **30**(6), 2263–2282 (2022)

[36] TAKEUCHI, Y., HARANGOZÓ, M., PEDRAZA, L., FLDI, T., KOZÁK, G., LI, Q., and BERÉNYI, A. Closed-loop stimulation of the medial septum terminates epileptic seizures. *Brain*, **144**(3), 885–908 (2021)

[37] STIEVE, B. J., RICHNER, T. J., KROOK-MAGNUSON, C., NETOFF, T. I., and KROOK-MAGNUSON, E. Optimization of closed-loop electrical stimulation enables robust cerebellar-directed seizure control. *Brain*, awac051 (2022)

[38] WYCKHUYS, T., RAEDT, R., VONCK, K., WADMAN, W., and BOON, P. Comparison of hippocampal deep brain stimulation with high (130Hz) and low frequency (5Hz) on afterdischarges in kindled rats. *Epilepsy Research*, **88**(2), 239–246 (2010)

[39] BRIEN, T. J., MORRIS, M. J., REID, C. A., JOVANOVSKA, V., BRIEN, P., VAN RAAY, L., GANDRATHI, A. K., and PINAULT, D. Rhythmic neuronal activity in S2 somatosensory and insular cortices contribute to the initiation of absence-related spike-and-wave discharges. *Epilepsia*, **53**(11), 1948–1958 (2012)

[40] NAMBU, A., TOKUNO, H., HAMADA, I., KITA, H., and HASEGAWA, N. Excitatory cortical inputs to pallidal neurons via the subthalamic nucleus in the monkey. *Journal of Neurophysiology*, **84**(1), 289–300 (2000)

[41] NAMBU, A., TAKADA, M., INASE, M., and TOKUNO, H. Dual somatotopical representations in the primate subthalamic nucleus: evidence for ordered but reversed body-map transformations from the primary motor cortex and the supplementary motor area. *Journal of Neuroscience*, **16**(8), 2671 (1996)

[42] EJ MÜLLER, ALBADA, S. V., KIM, J. W., and ROBINSON, P. A. Unified neural field theory of brain dynamics underlying oscillations in Parkinson's disease and generalized epilepsies. *Journal of Theoretical Biology*, **428**, 132–146 (2017)

[43] VAN ALBADA, S. J. and ROBINSON, P. A. Mean-field modeling of the basal ganglia-thalamocortical system, I: firing rates in healthy and parkinsonian states. *Journal of Theoretical Biology*, **257**(4), 642–663 (2009)

[44] VAN ALBADA, S. J., GRAY, R. T., DRYSDALE, P. M., and ROBINSON, P. A. Mean-field modeling of the basal ganglia-thalamocortical system, II: dynamics of parkinsonian oscillations. *Journal of Theoretical Biology*, **257**(4), 664–688 (2009)

[45] ROBINSON, P. A., RENNIE, C. J., and ROWE, D. L. Dynamics of large-scale brain activity in normal arousal states and epileptic seizures. *Physical Review E*, **65**(4), 041924 (2002)

[46] ROBINSON, P. A., RENNIE, C. J., WRIGHT, J. J., and BOURKE, P. D. Steady states and global dynamics of electrical activity in the cerebral cortex. *Physical Review E*, **58**(3), 3557 (1998)

[47] ROBINSON, P. A., RENNIE, C. J., and WRIGHT, J. J. Propagation and stability of waves of electrical activity in the cerebral cortex. *Physical Review E*, **56**(1), 826 (1997)

[48] FREYER, F., ROBERTS, J. A., BECKER, R., ROBINSON, P. A., RITTER, P., and BREAKSPEAR, M. Biophysical mechanisms of multistability in resting-state cortical rhythms. *Journal of Neuroscience*, **31**(17), 6353–6361 (2011)

[49] MARTEN, F., RODRIGUES, S., BENJAMIN, O., RICHARDSON, M. P., and TERRY, J. R. Onset of polyspike complexes in a mean-field model of human electroencephalography and its application to absence epilepsy. *Philosophical Transactions of the Royal Society A: Mathematical, Physical and Engineering Sciences*, **367**(1891), 1145–1161 (2009)

[50] ROBINSON, P. A., RENNIE, C. J., ROWE, D. L., and O'CONNOR, S. C. Estimation of multiscale neurophysiologic parameters by electroencephalographic means. *Human Brain Mapping*, **23**(1), 53–72 (2004)